A Detailed Reaction Mechanism for Thiosulfate Oxidation by Ozone in Aqueous Environments

Alexandra M. Deal[1], Alexander M. Prophet[1,2], Franky Bernal[1,2], Richard J. Saykally[1,2], and Kevin Wilson[1,*]

[1]*Chemical Sciences Division, Lawrence Berkeley National Laboratory, Berkeley, CA 94720*
[2]*Department of Chemistry, University of California, Berkeley, CA 94720*
**Corresponding Author; krwilson@lbl.gov*

TOC Figure

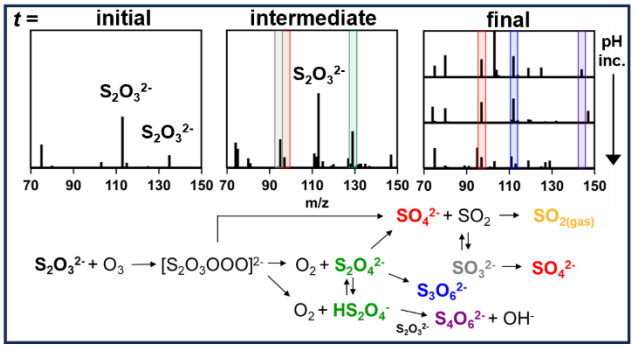

Abstract

The ozone oxidation, or ozonation, of thiosulfate is an important reaction for wastewater processing, where it is used for remediation of mining effluents, and for studying aerosol chemistry, where its fast reaction rate makes it an excellent model reaction. Although thiosulfate ozonation has been studied since the 1950's, challenges remain in developing a realistic reaction mechanism that can satisfactorily account for all observed products with a sequence of elementary reaction steps. Here, we present novel measurements using trapped microdroplets to study the pH-dependent thiosulfate ozonation kinetics. We detect known products and intermediates, including SO_3^{2-}, SO_4^{2-}, $S_3O_6^{2-}$, and $S_4O_6^{2-}$, establishing agreement with the literature. However, we identify $S_2O_4^{2-}$ as a new reaction intermediate, and find that the currently accepted mechanism does not directly explain observed pH effects. Thus, we develop a new mechanism, which incorporates $S_2O_4^{2-}$ as an intermediate and uses elementary steps to explain the pH-dependence of thiosulfate ozonation. The proposed mechanism is tested using a kinetic model benchmarked to the experiments presented here, then compared to literature data. We demonstrate good agreement between the proposed thiosulfate ozonation mechanism and experiments, suggesting that the insights in this paper can be leveraged in wastewater treatment and in understanding potential climate impacts.

Synopsis

This study addresses the pH-dependent ozone oxidation of thiosulfate, a reaction with applications in mining wastewater remediation and aerosol chemistry.

Keywords

Mining effluent, remediation, atmospheric aerosols, ozonation, polythionates, sulfur oxyions, pH-dependence

1. Introduction

Thiosalts, or incompletely oxidized sulfur compounds, have recently been classified as contaminants of emerging concern (CEC) due to their indirect aquatic toxicity. As such, a need for more complete thiosalt reaction mechanisms has been identified.[1] Thiosalts are formed in volcanic craters[2, 3] and hydrothermal vents[4] *via* the reaction between H_2S and SO_2 in aqueous environments (Figure 1A). They can also be formed in mines due to the incomplete oxidation of sulfur during the processing of sulfur-containing ores (Figure 1B) such as pyrite (FeS_2).[1, 5] Waste, often called “the tailing”, is transferred (Figure 1C) to tailing storage facilities (TSFs) and treated prior to release into the natural environment (Figure 1D). Typical thiosalt concentrations produced during mining operations are likely highly variable due to differences in mining practices and regulations, but one study by Rolia and Tan in 1985 measured concentrations from ~4 to 18 mM.[6] Due to their lack of direct toxicity, thiosalts are often left to naturally oxidize during storage, but sensitivity to the TSF environment can result in incomplete oxidization.[5, 7-9] When the TSF then releases the tailings, or is decommissioned, remaining thiosalts enter the environment, where further oxidation by air, bacteria, and sunlight is linked to increased acidic toxicity in natural waters.[1, 5, 8, 10-12] Furthermore, these TSFs can have poor regulation, which has led to catastrophic breaches (Figure 1E) including the Córrego do Feijão iron ore mine in Brazil.[13] As such, TSFs have recently come under scrutiny, and improved thiosalt oxidation processes may be required to meet new regulations.[14]

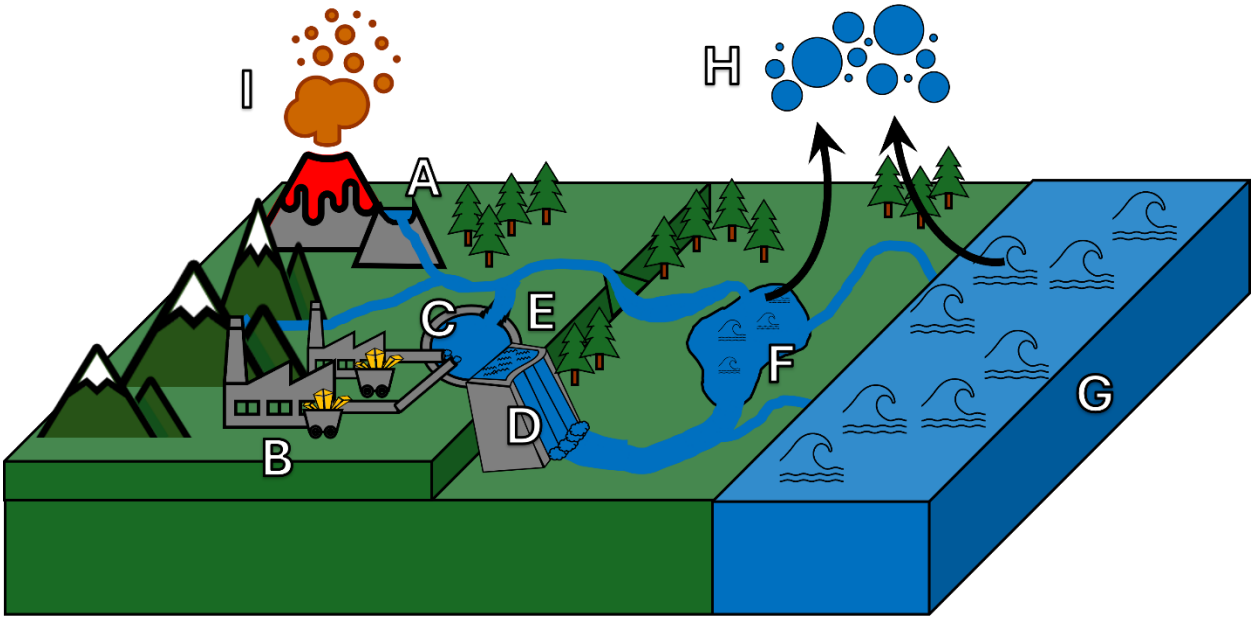

Figure 1. The lifecycle of thiosulfate in the environment. Thiosulfate, and other thiosalts, have been identified in (A) volcanic crater lakes,[2, 3] hydrothermal vents,[4] and (B) mining wastewater effluents.[1, 5] These effluents are typically transferred to tailings storage facilities (TSFs, C) where the wastewater is treated to remove known contaminants. After treatment, these wastewaters may be released to the natural environment (D), but there have also been TSF failures[13, 15] that have led to wastewater directly entering the environment (E). Sulfur species from volcanic run off (A), treated mining waters (D), and/or untreated mining waters (E) can then join large bodies of natural water such as lakes (F) and oceans (G), where breaking waves can create aqueous aerosols (H),[16] likely containing these sulfur species. Aerosols can persist for days to weeks,[17] exposing sulfur species to ozone and a variety of pH environments.[18] (I) Although it has not been directly investigated, H_2S and SO_2 emitted during volcanic eruptions[19] may form thiosulfate and other polythionates once incorporated in aqueous aerosols.

Thiosulfate ($S_2O_3^{2-}$), trithionate ($S_3O_6^{2-}$), and tetrathionate ($S_4O_6^{2-}$) are all common thiosalts in mining effluents, with thiosulfate being the most common.[5, 10] Recently, the use of ozone microbubbles for mining water treatment appears to be gaining momentum, with multiple recent laboratory and pilot studies,[9, 20, 21] but the currently accepted reaction mechanism is incomplete. Specifically, Takizawa et al.[22] demonstrated that the ozone oxidation of thiosulfate produces multiple products in neutral environments, but selectively produces sulfate in alkaline environments, which the currently accepted mechanism cannot fully explain. The exact speciation of thiosalts can be important for predicting environmental impacts, thus the role of pH in the ozone oxidation of thiosulfate must be better understood.[1, 5]

Thiosulfate is also used as a quenching agent in ozonation studies,[23] as a scavenger in ozone uptake studies,[24, 25] and its reaction with ozone is used to study aerosol chemistry.[26, 27] Aerosols, and their rich chemistry, remain one of the largest uncertainties in global climate modeling,[28] and the ozone oxidation of thiosulfate is fast, making it an excellent model reaction to study aerosol processing.[26, 27] In the natural environment, aqueous aerosols are formed by waves breaking over any large body of water (Figure 1F and G).[16] These aerosols can persist for days to weeks, undergoing several transformations, including changes in pH (Figure 1H).[18] Once in the atmosphere, fully oxidized thiosulfate (*i.e.*, sulfate) can have significant effects on climate forcing,[29] and incompletely oxidized thiosulfate may encounter ozone, resulting in the downstream production of sulfate.

Although it has not been directly investigated, thiosulfate may also form in long-lived (up to 3 years) stratospheric aerosols formed during volcanic eruptions, which will contain H_2S, SO_2, and water (Figure 1I).[19] Stratospheric aerosol injections (SAI), which mimic volcanic eruptions, have been proposed as a geoengineering effort to offset climate change, meaning the oxidation of thiosalts may have significant implications for any such SAIs. The pH-dependent reaction mechanism for the ozone oxidation of thiosulfate will thus be important for the mining community, the atmospheric chemistry community, and potential SAI designs.

The currently accepted reaction mechanism invokes three primary reaction steps:[22, 26, 27]

$$2\,S_2O_3^{2-} + O_3 + H_2O \rightarrow S_4O_6^{2-} + O_2 + 2OH^- \quad \text{R1}$$

$$S_2O_3^{2-} + O_3 \rightarrow S_2O_6^{2-} \quad \text{R2}$$

$$S_2O_3^{2-} + O_3 \rightarrow SO_4^{2-} + SO_2 \quad \text{R3}$$

SO_2 in water can then form bisulfite and sulfite *via* a coupled equilibrium:[30]

$$SO_2 + H_2O \rightleftarrows HSO_3^- + H^+ \rightleftarrows SO_3^{2-} + 2\,H^+, \quad \text{R4}$$

which is governed by the pKa of hydrated SO_2 (1.8) and the pKa of bisulfate (7.2).[30] Finally, sulfite can react with ozone to form sulfate or undergo a reversible disproportionation reaction with tetrathionate:[22, 27, 31]

$$S_4O_6^{2-} + SO_3^{2-} \rightleftarrows S_3O_6^{2-} + S_2O_3^{2-} \quad \text{R5}$$

However, this mechanism does not account for the pH-dependent product distributions demonstrated by Takizawa, et al.[22], instead requiring branching ratio assumptions between reactions R1-R3.

Furthermore, Hsu, et al.[27] showed that the reaction may be enhanced at droplet surfaces, which we hypothesize could be due to the surface enrichment of ozone. Ozone is relatively insoluble in bulk water but can be up to 100 times more concentrated at the water surface compared with the bulk.[32] Thus, bulk reactions between thiosulfate and ozone are likely diffusion-limited, while the overall mechanism is likely reaction-limited in environments with high surface-to-volume ratios (*e.g.,* ozone microbubble processing and atmospheric aerosols).

Here, we study the pH-dependent ozone oxidation of thiosulfate in levitated microdroplets, replicating the high surface-to-volume ratio of ozone microbubble processing and atmospheric aerosol environments. We study the reaction as a function of gas-phase ozone concentration and bulk-solution pH to replicate the varied mining and/or natural environments. Measured pH-dependent reaction kinetics are used to propose a new, more detailed mechanism for the ozone oxidation of thiosulfate and the proposed mechanism is benchmarked against the experiments presented here. Finally, the proposed mechanism is compared to prior literature data to ensure that the proposed mechanism explains both droplet and bulk chemistry.

2. Methods

2.1. Experiment

A quadrupole electrodynamic trap (QET) is used to trap and react arrays of microdroplets, which are then individually analyzed by mass spectrometry with an open-port sampling interface (OPSI-MS),[33-38] as previously utilized by Wilson and co-workers.[32, 34, 39, 40] As shown in Figure 2, the QET is housed in an environmentally controlled chamber and droplets are subjected to a constant flow (550 cm^3 min^{-1}) of humidified N_2, O_2, and O_3 at room temperature (295 K). Microdroplets are generated co-axially to the QET trapping rods by a piezo-electric dispenser (Microfab, MJ-ABP-01) with a 30 µm orifice and charged with a +450 V DC bias by an induction electrode immediately after generation. 10s to 100s of droplets can be trapped in the upper QET region and individually transferred to the lower QET region for sizing. Mie scattering is used to size the droplets by illuminating them with a 532 nm laser.[44]

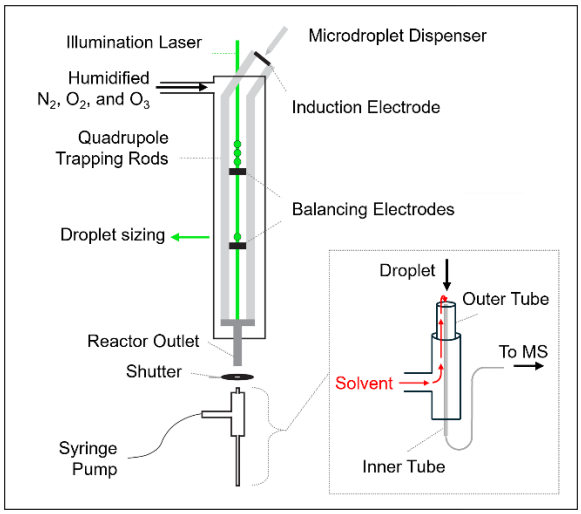

Figure 2. Experimental schematic of the quadrupole electrodynamic trap (QET) and (inset) the open-port sampling interface (OPSI) to the mass spectrometer. Adapted from Ref. [34] with permission from the Royal Society of Chemistry.

During an experiment, one droplet at a time is ejected from the QET, and the constant gas flow carries it to the open-port sampling interface (OPSI). The OPSI consists of an outer tube

connected to the solvent source and an axial inner tube leading to the mass spectrometer. The inner tube is connected to a Thermo-Fischer HESI-II heated-electrospray source, where sheath gas flow over the inner tube in the HESI creates a pressure differential, drawing the solvent and analyte into the analysis region of the Q Exactive Orbitrap mass spectrometer (Thermo Fischer Scientific, Inc.). The solvent delivery rate (typically ~4.5 mL h^{-1}) is slightly higher than the rate of solvent flow into the MS, creating a stable flow[33] and a small solvent pool that catches ejected microdroplets, dilutes their contents, and carries analytes to the MS.

Reference spectra of thiosulfate, sulfate, sulfite, tetrathionate, and trithionate in unreacted microdroplets were used to identify the characteristic ions, including fragmentation products, for each species (S1 in Supporting Information). Mass-to-charge ratios (m/z) for individual species are then tracked over time, providing a time-series of 'droplet detection events' (Figure S9 in the Supporting Information). Peak areas for each species are used to quantify the respective concentrations within the microdroplets; calibration curves at each pH for each species are shown in S2 in the Supporting Information.

The droplet chamber environment was controlled by a humidified mixture of O_2, O_3, and N_2. 10 cm^3 min^{-1} of oxygen was supplied to a corona discharge ozone generator and the resulting O_2/O_3 mixture was diluted into 2.5-5 L min^{-1} of nitrogen. 50 cm^3 min^{-1} of the diluted flow was combined with 500 cm^3 min^{-1} of humidified nitrogen, and the total flow (550 cm^3 min^{-1} of O_2, O_3, and N_2) was introduced to the QET. Before dispensing the droplets, the environmental chamber was equilibrated with the ozone generator off, which provided a humidified gas flow of up to 8 ppm O_2 in N_2. During reaction, droplets were exposed to a constant flow of 1-6 ppm of gas-phase ozone (O_3), measured by a UV ozone analyzer (2B Technologies, model 106-M). The gas flow is blocked from entering the OPSI except for ~4 s during droplet ejection events, and no indications of gas-phase chemistry within the ESI were observed.

2.2. Droplet Composition

Fresh solutions were prepared daily using HPLC-grade water (Sigma-Aldrich), $Na_2S_2O_3$ (Sigma-Aldrich, 99%), NaCl (Sigma-Aldrich, ≥99.5%), malonic acid (Sigma-Aldrich, 99%), L-glycine (≥99%), HCl (Sigma-Aldrich, 37%) and NaOH (Sigma-Aldrich, ≥98%). All droplets were dispensed from an aqueous 250 mM sodium thiosulfate ($Na_2S_2O_3$) solution, the lowest concentration that afforded a reasonable detection range throughout reactions. Solutions at pH 5 were buffered with 1 M malonic acid-NaOH and solutions at pH 9 were buffered with 1 M glycine-HCl. Buffers were chosen for their potential environmental relevance and effective buffering ranges. Reaction R3 and the subsequent hydrolysis of SO_2 described in the introduction suggest that up to two protons may be generated for each thiosulfate molecule consumed, meaning that up to 0.5 M H^+ could be produced. Buffer concentrations were therefore set to 1 M. Solutions with pH 13 were pH-adjusted using concentrated NaOH and were unbuffered due to the lack of viable buffers in this range. Regardless, no trithionate or tetrathionate were detected during the experiments, indicating no significant change in pH.[22] We also note that although glycine and OH^- will react with ozone,[41, 42] the rate constants and relative concentrations compared with thiosulfate are small enough that these reactions are negligible in these experiments, see S3 in Supporting Information.

The relative humidity in the QET was set to 95 ± 1% and measured at the beginning of each reaction. When the water activity of the droplets matched the relative humidity in the QET (a_w = 0.95), the dispenser produced droplets with r = 25 ± 1 μm. The pH 9 solution required ~300 mM NaCl to lower the water activity to the desired level; no additional salt was required for the pH 5 and pH 13 solutions. Droplet sizes did not significantly change throughout the reaction.

2.3. Kinetic Modeling

Kinetic mechanisms are benchmarked against experimental data using Kinetiscope©, a stochastic kinetics simulation software package, previously used by Wilson and co-workers.[43-45]

Kinetiscope© uses a Monte Carlo approach to simulating chemical kinetics where concentrations are propagated in time using the probabilities for each reaction step. The reaction mechanism is included as a series of discrete steps with rate constants and diffusion coefficients constrained by literature values (Table S3 in Supporting Information). Those not explicitly constrained by the literature are discussed here. When simulating reaction kinetics in microdroplets, we implement the geometric corrections developed by Willis, et al.[40] which account for surface-to-volume ratio and partitioning of solutes between the interface and the bulk (S5 in Supporting Information). Briefly, all species can adsorb to the water surface from the gas phase or from the bulk environment. Once adsorbed to the interface, species can react, desorb to the gas phase, or desorb into the bulk. The equilibrium values for the concentrations of adsorbed species are taken from literature where possible, and we employ Deep-UV Second Harmonic Generation (DUV-SHG) spectroscopy to directly probe thiosulfate, sulfite, and sulfate at the air-water interface (S4 in Supporting Information).

3. Experimental Results & Discussion

Ozone oxidation of thiosulfate (m/z = 113 and 135) was studied as a function of pH and gas-phase ozone concentration using levitated microdroplets as described in methods. Representative mass spectra are shown in Figure 3.

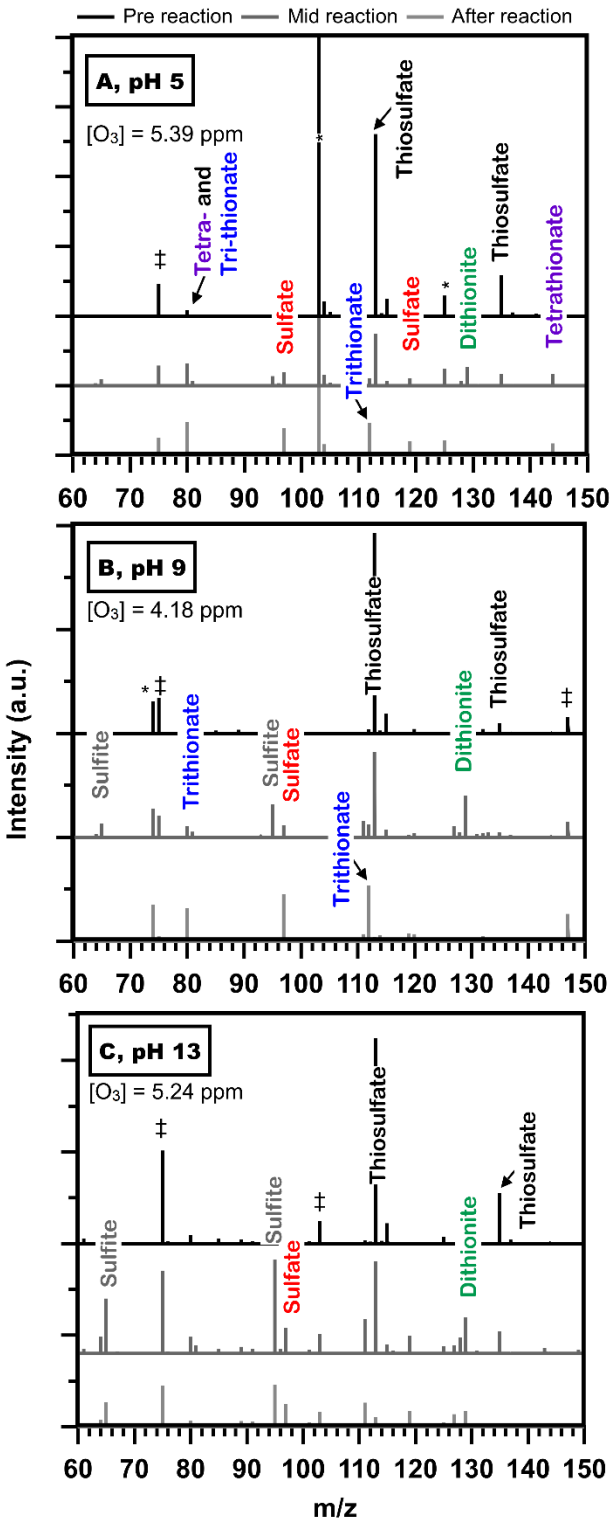

Figure 3. Representative mass spectra from the ozone oxidation of a 0.25 M thiosulfate solution at (A) pH 5, (B) pH 9, and (C) pH 13. Within each panel a mass spectrum is shown that is before reaction (t = 0 min, top), during reaction (t = 5 min, middle), and after reaction (t = 20 min, bottom). Spectra are offset along the y-axis for clarity. Species relevant to reaction kinetics are labeled with the common name; see S1 in Supporting Information for reference spectra with detailed

assignments of each peak and expanded reaction spectra. Colors are set to match those used in kinetics figures and reaction schemes. *indicates a buffer signal and ‡indicates a background signal.

Previous studies[22, 26, 27] identified sulfate (SO_4^{2-}), dithionate ($S_2O_6^{2-}$), trithionate ($S_3O_6^{2-}$), and tetrathionate ($S_4O_6^{2-}$) as reaction products and sulfite (SO_3^{2-}) as a reaction intermediate. Here, we identify SO_4^{2-} (m/z = 97 and 119), $S_3O_6^{2-}$ (m/z = 80, 112, 193, and 215), and $S_4O_6^{2-}$ (m/z = 80, 144, 225, and 247) as reaction products and SO_3^{2-} (m/z = 65 and 95) as a reaction intermediate, demonstrating consistency with prior studies. Additionally, we identify dithionite ($S_2O_4^{2-}$, m/z = 64) as a reaction intermediate, which had not been previously detected. However, the bulk-phase experiments performed by Takizawa, et al.[22] utilized titration to identify each of the known/expected products, and since dithionite is relatively unstable in aqueous environments with dissolved oxygen any dithionite formed likely decomposed before it could be identified. Similarly, the droplet experiments performed by Hsu, et al.[27] used Raman spectroscopy, which would not be able to distinguish dithionite from other sulfur oxyanion species. Thus, dithionite was likely present in both the bulk-phase Takizawa, et al.[22] and droplet Hsu, et al.[27] studies, but undetectable due to the methods used. Finally, we do not identify dithionate (expected m/z = 161 and 183) as a significant reaction product (S1 in Supporting Information). Mixed results in the literature[22, 26, 27] suggest that dithionate is only a minor product, if present at all, and thus will not be included in further discussions here.

Integrated OPSI-MS intensities converted to concentrations (S1 and S2 in Supporting Information) are used to asses product yields and sulfur loss (S9 in Supporting Information). The aqueous products measured here account for ~85% of the reacted sulfur at pH 5, ~60% of the reacted sulfur at pH 9, and ~65% of the reacted sulfur at pH 13. The remaining sulfur may be lost as gas-phase products (*e.g.*, SO_2), elemental sulfur, and/or experimental error [6, 22, 46] (S9 in

Supporting Information). Given that we cannot directly measure gas-phase products, we use the umbrella term 'S loss' to discuss SO_2 evaporation and any other loss mechanisms.

3.1. Reaction Kinetics

Reaction kinetics are obtained by analyzing a droplet every 1-2 minutes. Representative kinetic information for experiments with high ozone concentrations (5.39 ppm at pH 5, 4.18 ppm at pH 9 and 5.24 ppm at pH 13) are shown in Figure 4. Experiments (points) are compared with simulation results (lines), which will be discussed in Section 4. The first 20 minutes of reaction time are shown here for clarity; detailed reaction kinetics for all experiments are shown in S6 in Supporting Information.

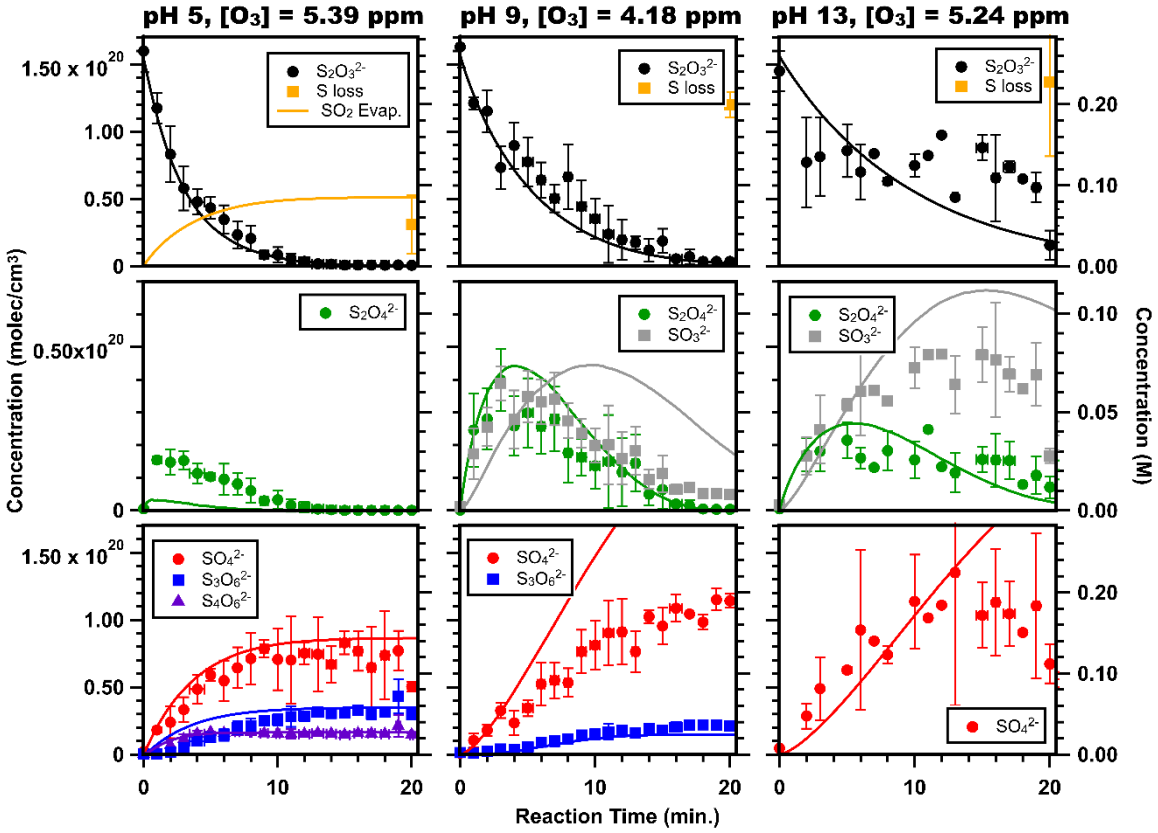

Figure 4. Representative detailed kinetics for the ozone oxidation of thiosulfate ($S_2O_3^{2-}$): thiosulfate decay (top panels), reaction intermediates (middle panels, y-scale zoomed for clarity) and reaction products (bottom panels) for pH 5 (left), pH 9 (middle) and pH 13 (right). Concentration is shown in molecular units on the left y-axes and in molar units on the right y-axis.

Experiment results are shown as points representing the average of 5 individual runs with error bars representing the standard deviation of each set. The net loss calculated *via* sulfur closure is shown as 'S loss' (orange circle) in the top panels; see S9 in Supporting Information for more details. Simulation results are shown as lines. The calculated amount of SO_2 lost to the gas phase is shown as an orange line in the top panel for pH 5. Green points and lines represent both $S_2O_4^{2-}$ and $HS_2O_4^-$ as these cannot be distinguished in experiments. Species not shown for a given pH were not detected at a significant concentration by experiments and were not predicted to form at a significant concentration by simulations.

Several qualitative features are observed. At early reaction times, thiosulfate is the limiting reactant, and thiosulfate decay is first order with respect to gas-phase ozone concentration (*i.e.,* increases linearly with ozone). This is shown by fitting the first 1-10 minutes of reaction data, shown in the top panels of Figure 4 and Figures S16-S19 in Supporting Information, with an 'initial thiosulfate decay rate'. The calculated initial thiosulfate decay rates shown in Figure 5 increase linearly with gas-phase ozone concentration. This is consistent with previous studies, which showed that the overall reaction rate is first order with respect to aqueous thiosulfate and gas-phase ozone concentrations.[24, 25] Figure 5 also shows that initial thiosulfate decay rates are inversely proportional to dispensed solution pH, which has not been explicitly noted in the literature and is not readily explained by the currently accepted mechanism (*e.g.*, R1-R3).

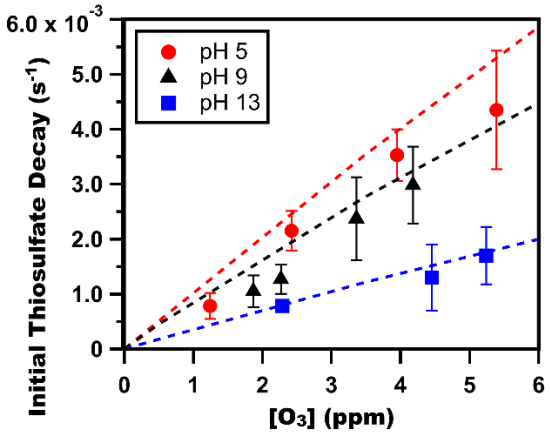

Figure 5. Initial thiosulfate decay rates as a function of ozone concentration at pH 5 (red circles), pH 9 (black triangles), and pH 13 (blue squares). Experimental initial decay rates (points) are extracted from the first ~5 minutes of reaction and averaged across 5 individual runs, with error

bars representing the standard deviation of each set. Simulation results are shown as dashed lines extended to zero. More detailed comparisons of thiosulfate decay kinetics as a function of ozone concentration at a given pH are shown in S6 in Supporting information.

Next, we discuss reaction intermediates (middle panels of Figure 4). $S_2O_4^{2-}$ (green) points represent the sum of $S_2O_4^{2-}$ and $HS_2O_4^-$ and SO_3^{2-} (grey) represent the sum of SO_3^{2-} and HSO_3^- as we cannot distinguish protonated forms from deprotonated forms in the mass spectra used here. We can, however, make some assumptions using the known pKa values for each species. Given that the pKa for dithionite is 2.44,[47] we do not expect a significant amount of $HS_2O_4^-$ to be present at any of the pH values studied here. However, the pKa for HSO_3^- is 7.2,[30] meaning a significant concentration of HSO_3^- could be present during pH 5 reactions although we cannot detect it (S1 in Supporting Information).

Regardless of exact speciation, a significant amount of dithionite ($S_2O_4^{2-}$) is detected across the pH values, and a significant amount of sulfite (SO_3^{2-}) is detected at pH 9 and pH 13. Sulfite is known to react rapidly with ozone to form sulfate[48] (SO_4^{2-}) but must compete with thiosulfate ($S_2O_3^{2-}$) for available ozone, slowing down its consumption while thiosulfate is still present. Dithionite ($S_2O_4^{2-}$) is not included in the currently accepted mechanism, but it is known to decompose in water with relatively slow reaction rates[47, 49] and decompose much faster with O_2.[50]

Finally, we discuss reaction product dependance on pH. Figure 3 and Figure 4 show that sulfate (SO_4^{2-}, red) is detected at all pH values, but tetrathionate ($S_4O_6^{2-}$, purple) is only detected at pH 5 and neither trithionate ($S_3O_6^{2-}$, blue) nor tetrathionate are detected at pH 13. This suggests that the formation of trithionate and tetrathionate are pH-dependent, which is consistent with the Takizawa, et al.[22] bulk studies. The currently accepted reaction mechanism invokes a disproportionation reaction between tetrathionate ($S_4O_6^{2-}$) and sulfite (SO_3^{2-}) to produce trithionate ($S_3O_6^{2-}$). This could explain the presence of trithionate at pH 5 but appears inconsistent with the pH 9 data, which shows trithionate without tetrathionate. Furthermore, we used ATR spectroscopy

to measure the disproportionation rate of tetrathionate and sulfite (S8 in Supporting Information), but the measured rate did not explain the kinetic trends shown in Figure 4 when included in the kinetic model.

3.2 Proposed mechanism

We propose a more detailed mechanism in Scheme 1, which includes the newly identified reaction intermediate, dithionite ($S_2O_4^{2-}$). The proposed mechanism is also pH-dependent, eliminating the need to assume branching ratios for R1-R3, includes a trithionate ($S_3O_6^{2-}$) production pathway that does not rely on tetrathionate ($S_4O_6^{2-}$) as a reaction intermediate, and includes a multistep tetrathionate production pathway instead of the single step invoked in R1.

Scheme 1. Proposed Mechanism for the Ozone Oxidation of Aqueous Thiosulfate ($S_2O_3^{2-}$).[a]

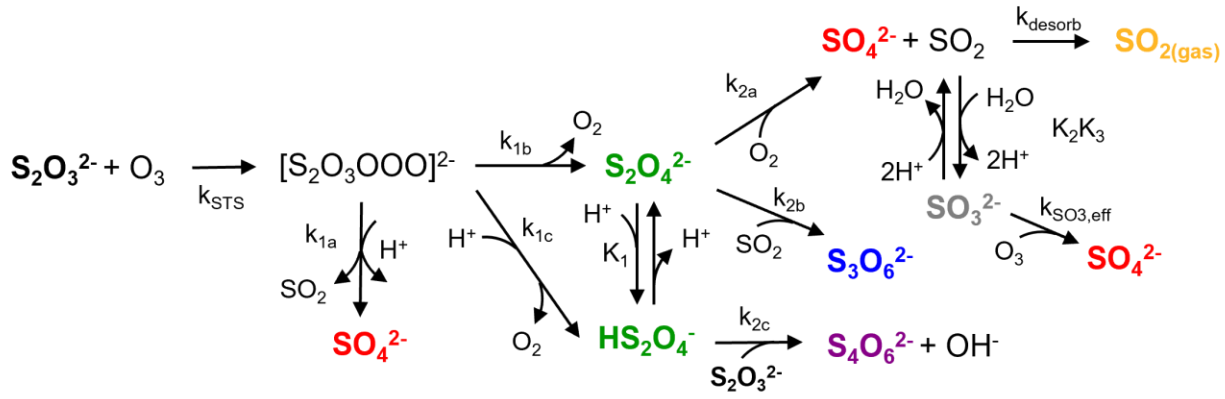

[a]Species detected in the experiments presented here are bolded and the font color is set to match the colors used in mass spectrum and kinetics figures. Although we cannot directly detect SO_2, its color is set to match that used when showing the calculated loss shown in kinetics figures.

Nucleophile-ozone adducts, called primary ozonides, are commonly identified in reactions with organics, and there is increasing evidence of their presence in inorganic reactions. Specifically, an ozonide intermediate has been observed for bromide ozonation,[51] invoked to explain the pH-dependance of iodide ozonation,[34] and calculated using *ab initio* methods for

sulfite ozonation.[52] By analogy, the first step in the mechanism proposed here is the formation of an ozone-thiosulfate adduct, $[O_3S_2OOO]^{2-}$, with potential structures and decay mechanisms based on the work of Liu, et al.[52] (S7 in Supporting Information). Using this framework, we write the subsequent reaction steps for thiosulfate plus ozone as:

$$[O_3S_2OOO]^{2-} \xrightarrow{k_{1b}} S_2O_4^{2-} + O_2 \quad \text{R6}$$

$$[O_3S_2OOOH]^{-} \xrightarrow{k_{1c}} HS_2O_4^{-} + O_2 \quad \text{R7}$$

Initial attempts at modeling the proposed mechanism showed that an additional pH-dependent source of SO_2 and SO_4^{2-} was needed to explain the rapid production of sulfate at early reaction times. Thus, we propose a third decomposition pathway, discussed further in S7 of Supporting Information:

$$O_3S_2OOO^{2-} + H^+ \xrightarrow{k_{1a}} SO_4^{2-} + SO_2 + H^+ \quad \text{R8}$$

Subsequent reaction steps are taken from the literature or inferred from stoichiometry and experimental results. $S_2O_4^{2-}$ and $HS_2O_4^-$ are a conjugate pair with pK_a = 2.44, denoted by K_1 in Scheme 1.[47] Aqueous dithionite is rapidly oxidized by oxygen, with rate constant k_{2a}, to form sulfate and SO_2.[50] SO_2 can evaporate, with rate constant k_{desorb}, or be solvated, forming pH-dependent coupled equilibria with bisulfite ($SO_2 + H_2O \rightleftarrows HSO_3^- + H^+$, pK_a = 1.8) and sulfite ($HSO_3^- \rightleftarrows SO_3^{2-} + H^+$, pK_a = 7.2), denoted K_2K_3.[30] Sulfite and bisulfite can both be further oxidized, with rate constant $k_{SO3,eff}$, by ozone to form sulfate (SO_4^{2-}).[48] In the absence of oxygen, $S_2O_4^{2-}$ is known to form trithionate ($S_3O_6^{2-}$) *via* multiple reactions with the final step:[49]

$$HS_2O_4^- + HSO_3^- \rightarrow S_3O_6^{2-} + H_2O \quad \text{R9}$$

However, it is unclear whether this is an elementary reaction step as two reactants with the same charge are likely to repel each other, and we observe only a weak dependance on pH for trithionate formation. Thus, we propose a similar reaction using the conjugates of $HS_2O_4^-$ and HSO_3^-:

$$S_2O_4^{2-} + SO_2 \xrightarrow{k_{2b}} S_3O_6^{2-}, \quad \text{R10}$$

which would have a complex pH-dependence. At pH 5, there is likely a mixture of $HS_2O_4^-$ and $S_2O_4^{2-}$ and a mixture of SO_2 and HSO_3^-, maybe even some SO_3^{2-}. As the pH increases to pH 9, the acid equilibria will shift so that there is more $S_2O_4^{2-}$, but less SO_2, resulting in similar overall reaction rates, which is consistent with the trithionate ($S_3O_6^{2-}$) production shown in Figure 4. As the pH further increases to pH 13, [SO_2] is likely negligible, shutting off trithionate production.

To our knowledge, the only relevant tetrathionate ($S_4O_6^{2-}$) formation mechanism in the literature is written as the stoichiometric reaction step R1.[22] This reaction step is difficult to model as it requires a third order rate constant, which has not been measured, and does not explain pH-dependent production of tetrathionate shown here. Thus, we propose:

$$HS_2O_4^- + S_2O_3^{2-} \xrightarrow{k_{2c}} S_4O_6^{2-} + OH^-, \quad \text{R11}$$

which would be affected by the pK_a of $HS_2O_4^-$ (2.44).

The proposed mechanism in Scheme 1 can be improved by future investigations targeting the proposed ozonide structures and the formation mechanisms for trithionate ($S_3O_6^{2-}$) and tetrathionate ($S_4O_6^{2-}$). Nevertheless, the proposed mechanism is largely based on known species

and reactions,[30, 47-50] incorporates much of the currently accepted chemistry,[22, 26, 27] and can better explain the pH-dependent ozone oxidation of thiosulfate ($S_2O_3^{2-}$).

4. Kinetic Modeling

4.1. Mechanism Viability

The proposed mechanism in Scheme 1 is incorporated into the Kinetiscope© model and reaction conditions (*e.g.*, $[O_{3(gas)}]$ and $[S_2O_3^{2-}]_0$) are set to match those used in experiments. All rate constants are constrained by literature values (Table S3 in Supporting Information) except k_{1b}, k_{2b}, and k_{2c}, corresponding to reactions R6, R10, and R11, respectively, which are fit to the experimental data presented here (S10 in Supporting Information).

Simulated pH-dependent results (Figure 4), simulated ozone-dependent results (S6 in Supporting Information), and simulated initial rates of thiosulfate decay (Figure 5) all agree with experiments, especially for pH 5, pH 9, and at higher ozone concentrations. The simulated thiosulfate decay kinetics deviate slightly from experimental values for pH 13 and for pH 9 with low ozone concentrations ($[O_{3(gas)}]$ < 3 ppm), which may be linked to sulfur loss mechanisms not accounted for by the proposed mechanism (S9 in Supporting Information) and by decreased experimental accuracy at long reaction times. On the other hand, the simulation reproduces the shape of the dithionite ($S_2O_4^{2-}$) intermediate kinetics (Figure 4, middle panels, green) at all three pH values, which provides significant confidence in the proposed mechanism, where $S_2O_4^{2-}$ and $HS_2O_4^-$ have a significant role. As mentioned previously, we are unable to detect HSO_3^- using OPSI-MS, and attempts to record reference spectra for dithionite ($S_2O_4^{2-}$) demonstrated that dithionite rapidly decomposes to form sulfite (SO_3^{2-}), possibly even within the OPSI-MS. Despite this, the simulation and experimental results for pH 13 agree, and the pH 5 simulation calculated negligible concentrations of sulfite (SO_3^{2-}) and bisulfite (HSO_3^-), suggesting that our insensitivity to bisulfite does not interfere with the overall kinetic understanding.

Simulation and experimental results also show reasonable agreement for trithionate ($S_3O_6^{2-}$), and tetrathionate ($S_4O_6^{2-}$) production across all three pH values and for sulfate (SO_4^{2-}) production at pH 5. Deviations for sulfate kinetics at pH 9 and pH 13 are likely due to limitations in modeling SO_2 evaporation and equilibria (S5.3 in Supporting Information). We find that the final concentration of sulfate (SO_4^{2-}) is sensitive to the kinetics of SO_2 and the simple kinetic modeling of SO_2 used here likely does not fully capture its behavior. Regardless, the simulation shows good agreement for pH 5 and acceptable agreement for pH 9 and pH 13. The simulation also shows close agreement with experiments for the other products, trithionate ($S_3O_6^{2-}$) and tetrathionate ($S_4O_6^{2-}$). Specifically, the simulation accurately captures the kinetics and final concentration at pH values where these products are observed and accurately predicts negligible concentrations for each at pH values where these products are not observed.

Overall, the proposed mechanism accurately captures the kinetics of the ozone oxidation of thiosulfate experiments presented here, and predicts kinetic changes due to pH, which could not be explained using the previously accepted mechanism.

4.2. Comparison with Other Experiments

We compare the proposed mechanism in Scheme 1 to literature data for the ozone oxidation of thiosulfate in bulk solution[22] and ~3 um droplets.[27] Takizawa, et al.[22] studied the bulk ozone oxidation of thiosulfate by bubbling mixed O_2/O_3 through the reaction vessel and extracting aliquots every 30 minutes for analysis. The reaction was studied in a neutral pH-unadjusted solution and in alkaline solution as shown in Figure 6.

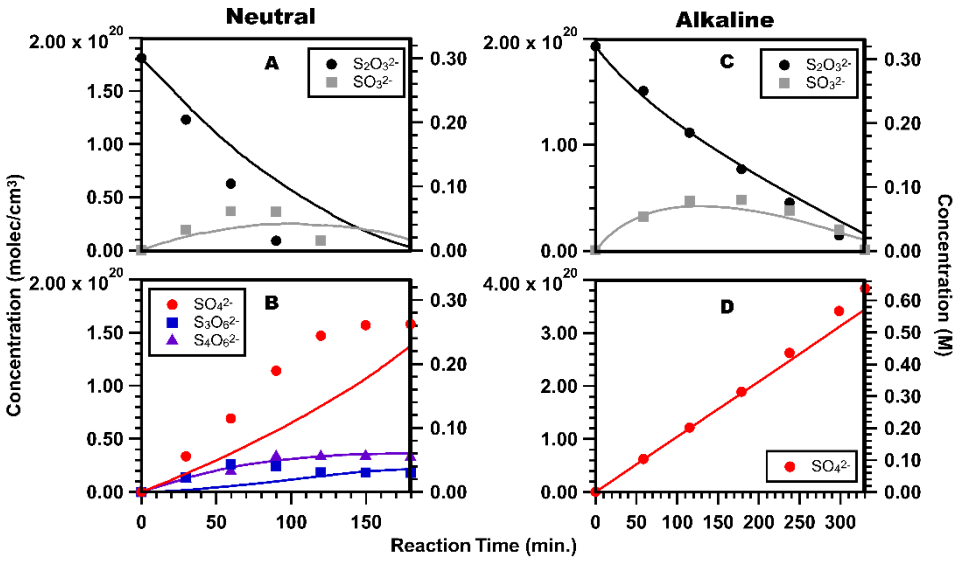

Figure 6. Bulk kinetics for the ozone oxidation of thiosulfate ($S_2O_3^{2-}$) in neutral (A & B) and alkaline (C & D) solution from Takizawa, et al.[22] Thiosulfate and sulfite kinetics are shown in the top panels, and product kinetics are shown in the bottom panels. Concentration is shown in molecular units on the left y-axes and in molar units on the right y-axis. Experimental data (points) are reproduced from Takizawa, et al.[22] No trithionate ($S_3O_6^{2-}$) or tetrathionate ($S_4O_6^{2-}$) was detected under bulk alkaline conditions. The neutral solution was pH-unadjusted and the alkaline solution pH-adjusted with added NaOH equal to or greater than the amount of acid produced during reaction.[22] Simulation results from this work are shown as lines.

Simulation results (lines) using the proposed mechanism in Scheme 1 and experimental parameters from Takizawa, et al.[22] ($[O_{3(gas)}]$ and $[S_2O_3^{2-}]_0$) are also shown in Figure 6. We use the same bulk reaction steps and rates as Section 4.1 (shown as reaction steps B1-B10 in Table S3 in Supporting Information), except for the rate constants for reaction steps R10 (k_{2b}) and R11 (k_{2c}) when simulating the neutral data (Figure 6, A & B). The Takizawa, et al.[22] solutions were not buffered, and the authors note that over the course of the reaction, the pH of the 'neutral' solution changed dramatically, dropping to pH 1-2, which corresponds to a 5- to 6- order of magnitude decrease in $[H^+]$. Although the mechanism proposed here is pH-dependent, explicitly modeling pH is computationally expensive due to the low concentrations of H^+ relative to other reactants. We circumvent this issue by using a steady-state assumption for $[H^+]$, which is accurate for our buffered solutions but will not adequately represent kinetics in these unbuffered solutions.

We thus use 'effective' rates for trithionate ($S_3O_6^{2-}$) and tetrathionate ($S_4O_6^{2-}$) production and find that using $k_{2b}^{eff} = 1\,x\,10^{-16} cm^3 \cdot molec^{-1} \cdot s^{-1}$ and $k_{2c}^{eff} = 3\,x\,10^{-17} cm^3 \cdot molec^{-1} \cdot s^{-1}$ for reactions R10 and R11, respectively, adequately reproduce the Takizawa, et al.[22] experiments (Figure 6B). To explain the difference in these effective rates, we discuss how changing pH would affect trithionate and tetrathionate production. As the pH decreases from 7 to 1, [$HS_2O_4^-$] will increase, resulting in the higher k_{2c}^{eff} used here. Similarly, [SO_2] will increase, which could increase trithionate production. However, the pKa of $HS_2O_4^-$ is higher (2.44)[47] than that of solvated aqueous SO_2 (1.8),[30] meaning that $\Delta[S_2O_4^{2-}]$ is likely greater than $\Delta[SO_2]$ resulting in the lower k_{2b}^{eff} used here.

In alkaline solution (Figure 6, C & D), the pH likely does not significantly change, as NaOH was added in sufficient concentrations to neutralize any acidification due to reaction.[22] We assume the alkaline solution to be at pH 13 for simulations given the similarities in product yields between the alkaline Takizawa, et al.[22] experiment (Figure 6, C & D) and the pH 13 experiments presented here (Figure 4, right column). Thus, simulations of the bulk alkaline data accurately capture reaction kinetics using the same rate constants used in Section 4.1. Despite uncontrolled pH in the Takizawa, et al.[22] experiments, the simulation results shown in Figure 6 accurately predict the bulk kinetics using the proposed mechanism with effective rate constants, especially early times when the pH changes are small.

Finally, we compare our proposed mechanism with the trapped droplet experiments from Hsu, et al.[27] Compared with our experiments, Hsu, et al.[27] study the ozone oxidation of thiosulfate in much smaller droplets (~25 μm vs. up to 4 μm). Given the enhanced role of geometry in smaller droplets, a complete analysis of the Hsu, et al.[27] data using our simulations is beyond the scope of this paper and will be included in future work exploring interfacial effects. Here, we test the simulation against one data set from Hsu, et al.[27], finding reasonable agreement between the experiments and model (S11 in Supporting Information).

4.3. Model Insights

Kinetic modeling offers additional insights into the reaction mechanism. First, thiosulfate ($S_2O_3^{2-}$) decay during ozonation is decoupled from downstream reactions at higher pH values but is heavily modulated by tetrathionate production (Reaction R11 labeled with k_{2c} in Scheme 1) at lower pH values. Tetrathionate production is in direct competition with the acid/base equilibrium of $HS_2O_4^-$ to $S_2O_4^{2-}$, which has a pKa (2.44).[47] However, [$S_2O_3^{2-}$] is much larger than [$HS_2O_4^-$] at the pH values studied here, resulting in overall reaction rates that favor tetrathionate production at pH 5 (Figure 4) and pH 7 (Figure 6), which affects the overall reaction stoichiometry. Specifically, simulations show that thiosulfate and ozone molecules are consumed in a 1:1 ratio at pH 9 and 13, where R11 is shut off, but in a 1.1:1 ratio at pH 5, where R11 is active.

Second, anoxic $S_2O_4^{2-}$ decomposition occurs too slowly to explain the observed kinetics but incorporating the oxygen-assisted decomposition of $S_2O_4^{2-}$ in the kinetic model matches the observed kinetics. This means that dissolved oxygen can also modulate the ozone oxidation of thiosulfate, changing product yields.

Finally, it is worth noting that the ozone oxidation of thiosulfate may be mediated by air-water interfaces. In particular, the proposed reaction mechanism involves three species (O_3, O_2, and SO_2) that will have gas-interface-bulk diffusion equilibria coupled with their reaction kinetics. Significant work has been performed to understand reaction-diffusion equilibria for ozone as a reactant,[32] but future work can focus on other gases, especially those that act as reactive intermediates.

5. Environmental Implications

Using OPSI-MS to probe the reaction of thiosulfate and ozone in droplets over time provided a new level of detail regarding the reaction kinetics. We directly identified an additional reaction intermediate, dithionite ($S_2O_4^{2-}$), and proposed a new pH-dependent reaction mechanism, which can be used to understand product speciation. Kinetic modeling of the proposed mechanism

demonstrated excellent agreement with the droplet experiments presented here, literature droplet experiments,[27] and literature bulk experiments.[22] The proposed mechanism is thus relevant to the ozone oxidation of thiosulfate in both droplet and bulk phases.

The data presented here and bulk data from Takizawa, et al.[22] show that product distributions vary with solution pH. Namely, in both droplet and bulk phases, highly alkaline environments selectively form sulfate (Figure 4, right panel, and Figure 6D), while environments with pH ≤ 9 also form trithionate and tetrathionate (Figure 4, left and middle panels, and Figure 6B). This will be important to note when treating mining wastewater with ozone microbubbles as the final thiosalt speciation can be important for understanding environmental impacts.[1, 5] For example, wastewater will be pH-adjusted prior to release into natural waters, but if any incompletely oxidized sulfur remains when the wastewater is released, it will then oxidize and acidify the receiving water.

Breaking waves on large bodies of water like oceans and lakes that contain thiosalts, either from natural or anthropogenic sources, may create atmospheric aerosols containing these same thiosalts.[16] Given the predicted acidity of atmospheric aerosols,[18] this study suggests that ozone oxidation of thiosulfate in aerosols will create a mixture of completely oxidized sulfur (*i.e.*, sulfate) and incompletely oxidized sulfur (*i.e.,* trithionate and tetrathionate). The incompletely oxidized sulfur could then be deposited back into natural waters where other oxidation mechanisms would result in acidification of those receiving waters.[1, 5, 8, 10-12] Similar analyses could also be used to better understand the climate effects of volcanic eruptions,[19] which could create thiosulfate in stratospheric aerosols, and would have implications for SAIs designed to mimic volcanic climate effects.

Regardless of the source of thiosulfate or other thiosalts, their metastable nature means that they could be transported far from their origin before undergoing oxidation. This delay may cause unexpected downstream natural water acidification, and thus ecological toxicity,[1, 5, 8, 10-12] and create unexpected sulfate aerosols, which have a significant effect on climate forcing.[29] Testing

for thiosalts in groundwaters can be challenging,[2, 4, 5] and, to our knowledge, field campaigns have not been able to directly identify thiosalts in either tropospheric or stratospheric aerosols Difficulties in distinguishing sulfur species in complex mixtures[53] suggest that thiosalts may be a previously unidentified temporary sink for reactive sulfur in the environment, and more direct detection studies will be required to understand the full implications of the reaction mechanism presented here.

Acknowledgements: This work was supported by the Condensed Phase and Interfacial Molecular Science Program (CPIMS), in the Chemical Sciences Geosciences and Biosciences Division of the Office of Basic Energy Sciences of the U.S. Department of Energy under Contract No. DE-AC02-05CH11231. We thank Professor Yuan-Pin Chang for providing the data in Figure S27.

Supporting Information:

Reference Mass Spectra & Droplet Events; Calibration Curves; Ozone Reactions; DUV-SHG; Kinetic Modeling Information; Detailed Kinetics for All Experiments; Proposed Intermediate Structures; Kinetics of Tetrathionate and Sulfate Disproportionation; Product Yields and Sulfur Loss; Fitting Procedure for k_{1b}, k_{2b}, and k_{2c}; Model Comparison with Hsu, *et al*.

References

(1) Neculita, C. M.; Coudert, L.; Rosa, E.; Mulligan, C. N. Future prospects for treating contaminants of emerging concern in water and soils/sediments. In *Advanced Nano-Bio Technologies for Water and Soil Treatment*, Filip, J., Cajthaml, T. N., Petra, Černík, M., Zbořil, R. Eds.; Springer, 2020; pp 589-605.
(2) Casas, A. S.; Armienta, M. A.; Ramos, S. Sulfur speciation with high performance liquid chromatography as a tool for El Chichón volcano, crater lake monitoring. *J. South Am. Earth Sci.* **2016**, *72*, 241-249.
(3) Rowe Jr, G. L.; Brantley, S. L.; Fernandez, M.; Fernandez, J. F.; Borgia, A.; Barquero, J. Fluid-volcano interaction in an active stratovolcano: the crater lake system of Poás volcano, Costa Rica. *J. Volcanol. Geotherm. Res.* **1992**, *49* (1-2), 23-51.
(4) Xu, Y.; Schoonen, M.; Nordstrom, D. K.; Cunningham, K.; Ball, J. Sulfur geochemistry of hydrothermal waters in Yellowstone National Park: I. The origin of thiosulfate in hot spring waters. *Geochim. Cosmochim. Acta* **1998**, *62* (23-24), 3729-3743.
(5) Miranda-Trevino, J. C.; Pappoe, M.; Hawboldt, K.; Bottaro, C. The importance of thiosalts speciation: review of analytical methods, kinetics, and treatment. *Crit. Rev. Env. Sci. Technol.* **2013**, *43* (19), 2013-2070.
(6) Rolia, E.; Chakrabarti, C. L. Kinetics of decomposition of tetrathionate, trithionate, and thiosulfate in alkaline media. *Environ. Sci. Technol.* **1982**, *16* (12), 852-857.
(7) Kuyucak, N. Management of thiosalts in mill effluents by chemical oxidation or buffering in the lime neutralization process. *Miner. Eng.* **2014**, *60*, 41-50.
(8) Dinardo, O.; Salley, J. *Treatment of Thiosalts in Milling Effluents: A Review of Treatment Processes*; Report presented for Thiosalts Consortium - Phase II, Report CANMENT-MMSL 97-060 (CR); CANMET Mining and Mineral Sciences Laboratories, Ottawa, ON, Canada, 1998.
(9) Gervais, M.; Dubuc, J.; Paquin, M.; Gonzalez-Merchan, C.; Genty, T.; Neculita, C. M. Comparative efficiency of three advanced oxidation processes for thiosalts oxidation in mine-impacted water. *Miner. Eng.* **2020**, *152*, 106349.
(10) Ryskie, S.; Neculita, C. M.; Rosa, E.; Coudert, L.; Couture, P. Active treatment of contaminants of emerging concern in cold mine water using advanced oxidation and membrane-related processes: a review. *Minerals* **2021**, *11* (3), 259.
(11) Schwartz, M.; Vigneault, B.; McGeer, J. *Evaluating the potential for thiosalts to contribute to toxicity in mine effluents*; Report presented for Thiosalts Consortium, Project: 602591, Report CANMET-MMSL 06-053 (CR); CANMET Mining and Mineral Sciences Laboratories, 2007.
(12) Fahd, F.; Khan, F.; Hawboldt, K.; Abbassi, R. Developing a novel methodology for ecological risk assessment of thiosalts. *Stochastic Environ. Res. Risk Assess.* **2014**, *28*, 383-391.
(13) Buch, A. C.; Sims, D. B.; de Ramos, L. M.; Marques, E. D.; Ritcher, S.; Abdullah, M. M.; Silva-Filho, E. V. Assessment of environmental pollution and human health risks of mine tailings in soil: after dam failure of the Córrego do Feijão Mine (in Brumadinho, Brazil). *Environ. Geochem. Health* **2024**, *46* (3), 72.
(14) New Global Industry Standard on Tailings Management aims to improve the safety of tailings facilities in the mining industry; https://www.icmm.com/en-gb/news/2020/new-global-industry-standard-on-tailings-management
(15) Achterberg, E. P.; Braungardt, C.; Morley, N. H.; Elbaz-Poulichet, F.; Leblanc, M. Impact of Los Frailes mine spill on riverine, estuarine and coastal waters in southern Spain. *Water Res.* **1999**, *33* (16), 3387-3394.
(16) May, N. W.; Gunsch, M. J.; Olson, N. E.; Bondy, A. L.; Kirpes, R. M.; Bertman, S. B.; China, S.; Laskin, A.; Hopke, P. K.; Ault, A. P. Unexpected contributions of sea spray and lake spray aerosol to inland particulate matter. *Environ. Sci. Technol. Lett.* **2018**, *5* (7), 405-412.
(17) Dobson, C. M.; Ellison, G. B.; Tuck, A. F.; Vaida, V. Atmospheric aerosols as prebiotic chemical reactors. *Proc. Natl. Acad. Sci.* **2000**, *97* (22), 11864-11868.
(18) Griffith, E. C.; Tuck, A. F.; Vaida, V. Ocean–atmosphere interactions in the emergence of complexity in simple chemical systems. *Accounts Chem. Res.* **2012**, *45* (12), 2106-2113.

(19) Robock, A. Climatic impacts of volcanic eruptions. In *The encyclopedia of volcanoes*, Elsevier, 2015; pp 935-942.
(20) Khuntia, S.; Majumder, S. K.; Ghosh, P. Removal of ammonia from water by ozone microbubbles. *Ind. Eng. Chem. Res.* **2013**, *52* (1), 318-326.
(21) Ryskie, S.; Gonzalez-Merchan, C.; Neculita, C. M.; Genty, T. Efficiency of ozone microbubbles for ammonia removal from mine effluents. *Miner. Eng.* **2020**, *145*, 106071.
(22) Takizawa, M.; Okuwaki, A.; Okabe, T. The chemical behavior of low valence sulfur compounds. VIII. the oxidation of sodium thiosulfate with ozone. *Bull. Chem. Soc. Jpn.* **1973**, *46* (12), 3785-3789.
(23) Atkinson, A. J.; Ray, H.; Wert, E. C. Efficiency of Ozone Quenching Agents at Different Temperature, pH, and Hydrodynamic Conditions. *Ozone: Sci. Eng.* **2024**, 1-20.
(24) Kanofsky, J. R.; Sima, P. D. Reactive absorption of ozone by aqueous biomolecule solutions: implications for the role of sulfhydryl compounds as targets for ozone. *Arch. Biochem. Biophys.* **1995**, *316* (1), 52-62.
(25) Müller, B.; Heal, M. R. The mass accommodation coefficient of ozone on an aqueous surface. *Phys. Chem. Chem. Phys.* **2002**, *4* (14), 3365-3369. DOI: 10.1039/b202491h
(26) Enami, S.; Vecitis, C.; Cheng, J.; Hoffmann, M.; Colussi, A. Electrospray mass spectrometric detection of products and short-lived intermediates in aqueous aerosol microdroplets exposed to a reactive gas. *J. Phys. Chem. A* **2007**, *111* (50), 13032-13037.
(27) Hsu, S.-H.; Lin, F.-Y.; Huang, G. G.; Chang, Y.-P. Accelerated Sulfur Oxidation by Ozone on Surfaces of Single Optically Trapped Aerosol Particles. *J. Phys. Chem. C* **2023**, *127* (13), 6248-6261. DOI: 10.1021/acs.jpcc.2c06831
(28) Watson-Parris, D.; Smith, C. J. Large uncertainty in future warming due to aerosol forcing. *Nat. Clim. Change* **2022**, *12* (12), 1111-1113.
(29) Penner, J.; Chuang, C.; Grant, K. Climate forcing by carbonaceous and sulfate aerosols. *Clim. Dyn.* **1998**, *14*, 839-851.
(30) Erickson, R. E.; Yates, L. M.; Clark, R. L.; McEwen, D. The reaction of sulfur dioxide with ozone in water and its possible atmospheric significance. *Atmos. Environ.* **1977**, *11* (9), 813-817.
(31) Varga, D.; Horváth, A. K. Kinetics and mechanism of the decomposition of tetrathionate ion in alkaline medium. *Inorg. Chem.* **2007**, *46* (18), 7654-7661.
(32) Willis, M. D.; Wilson, K. R. Coupled Interfacial and Bulk Kinetics Govern the Timescales of Multiphase Ozonolysis Reactions. *J. Phys. Chem. A* **2022**, *126* (30), 4991-5010. DOI: 10.1021/acs.jpca.2c03059
(33) Kaur Kohli, R.; Van Berkel, G. J.; Davies, J. F. An Open Port Sampling Interface for the Chemical Characterization of Levitated Microparticles. *Anal. Chem.* **2022**, *94* (8), 3441-3445. DOI: 10.1021/acs.analchem.1c05550
(34) Prophet, A. M.; Polley, K.; Van Berkel, G. J.; Limmer, D. T.; Wilson, K. R. Iodide oxidation by ozone at the surface of aqueous microdroplets. *Chem. Sci.* **2024**, *15* (2), 736-756. DOI: 10.1039/d3sc04254e
(35) Liu, C.; Van Berkel, G. J.; Kovarik, P.; Perot, J. B.; Inguva, V.; Covey, T. R. Fluid Dynamics of the Open Port Interface for High-Speed Nanoliter Volume Sampling Mass Spectrometry. *Anal. Chem.* **2021**, *93* (24), 8559-8567. DOI: 10.1021/acs.analchem.1c01312
(36) Van Berkel, G. J.; Kertesz, V. An open port sampling interface for liquid introduction atmospheric pressure ionization mass spectrometry. *Rapid Commun. Mass Spectrom.* **2015**, *29* (19), 1749-1756. DOI: 10.1002/rcm.7274
(37) Kaur Kohli, R.; Reynolds, R. S.; Wilson, K. R.; Davies, J. F. Exploring the influence of particle phase in the ozonolysis of oleic and elaidic acid. *Aerosol Sci. Tech.* **2024**, *58* (4), 356-373.
(38) Cahill, J. F.; Riba, J.; Kertesz, V. Rapid, untargeted chemical profiling of single cells in their native environment. *Anal. Chem.* **2019**, *91* (9), 6118-6126.
(39) Jacobs, M. I.; Davies, J. F.; Lee, L.; Davis, R. D.; Houle, F.; Wilson, K. R. Exploring Chemistry in Microcompartments Using Guided Droplet Collisions in a Branched Quadrupole Trap Coupled to a Single

Droplet, Paper Spray Mass Spectrometer. *Anal. Chem.* **2017**, *89* (22), 12511-12519. DOI: 10.1021/acs.analchem.7b03704
(40) Willis, M. D.; Rovelli, G.; Wilson, K. R. Combining Mass Spectrometry of Picoliter Samples with a Multicompartment Electrodynamic Trap for Probing the Chemistry of Droplet Arrays. *Anal. Chem.* **2020**, *92* (17), 11943-11952. DOI: 10.1021/acs.analchem.0c02343
(41) Berger, P.; Leitner, N. K. V.; Doré, M.; Legube, B. Ozone and hydroxyl radicals induced oxidation of glycine. *Water Res.* **1999**, *33* (2), 433-441.
(42) Merényi, G.; Lind, J.; Naumov, S.; von Sonntag, C. The reaction of ozone with the hydroxide ion: mechanistic considerations based on thermokinetic and quantum chemical calculations and the role of HO4− in superoxide dismutation. *Chem. Eur. J.* **2010**, *16* (4), 1372-1377.
(43) Heine, N.; Houle, F. A.; Wilson, K. R. Connecting the elementary reaction pathways of criegee intermediates to the chemical erosion of squalene interfaces during ozonolysis. *Environ. Sci. Technol.* **2017**, *51* (23), 13740-13748.
(44) Houle, F. A.; Wiegel, A. A.; Wilson, K. R. Predicting aerosol reactivity across scales: from the laboratory to the atmosphere. *Environ. Sci. Technol.* **2018**, *52* (23), 13774-13781.
(45) Wilson, K. R.; Prophet, A. M.; Rovelli, G.; Willis, M. D.; Rapf, R. J.; Jacobs, M. I. A kinetic description of how interfaces accelerate reactions in micro-compartments. *Chem. Sci.* **2020**, *11* (32), 8533-8545. DOI: 10.1039/d0sc03189e
(46) Mizoguchi, T.; Takei, Y.; Okabe, T. The chemical behavior of low valence sulfur compounds. X. Disproportionation of thiosulfate, trithionate, tetrathionate and sulfite under acidic conditions. *Bull. Chem. Soc. Jpn.* **1976**, *49* (1), 70-75.
(47) Wayman, M.; Lem, W. Decomposition of aqueous dithionite. Part II. A reaction mechanism for the decomposition of aqueous sodium dithionite. *Can. J. Chem.* **1970**, *48* (5), 782-787.
(48) Hoigné, J.; Bader, H.; Haag, W.; Staehelin, J. Rate constants of reactions of ozone with organic and inorganic compounds in water—III. Inorganic compounds and radicals. *Water Res.* **1985**, *19* (8), 993-1004.
(49) Kovacs, K. M.; Rabai, G. Mechanism of the oscillatory decomposition of the dithionite ion in a flow reactor. *Chem. Commun.* **2002**, (7), 790-791. DOI: 10.1039/b200981a
(50) Rinker, R. G.; Gordon, T. P.; Mason, D. M.; Sakaida, R. R.; Corcoran, W. H. Kinetics and mechanism of the air oxidation of the dithionite ion (S2O4=) in aqueous solution. *J. Phys. Chem.* **1960**, *64* (5), 573-581.
(51) Artiglia, L.; Edebeli, J.; Orlando, F.; Chen, S.; Lee, M. T.; Corral Arroyo, P.; Gilgen, A.; Bartels-Rausch, T.; Kleibert, A.; Vazdar, M.; Andres Carignano, M.; Francisco, J. S.; Shepson, P. B.; Gladich, I.; Ammann, M. A surface-stabilized ozonide triggers bromide oxidation at the aqueous solution-vapour interface. *Nat. Commun.* **2017**, *8* (1), 700. DOI: 10.1038/s41467-017-00823-x
(52) Liu, Q.; Schurter, L. M.; Muller, C. E.; Aloisio, S.; Francisco, J. S.; Margerum, D. W. Kinetics and mechanisms of aqueous ozone reactions with bromide, sulfite, hydrogen sulfite, iodide, and nitrite ions. *Inorg. Chem.* **2001**, *40* (17), 4436-4442.
(53) Dovrou, E.; Lim, C. Y.; Canagaratna, M. R.; Kroll, J. H.; Worsnop, D. R.; Keutsch, F. N. Measurement techniques for identifying and quantifying hydroxymethanesulfonate (HMS) in an aqueous matrix and particulate matter using aerosol mass spectrometry and ion chromatography. *Atmos. Meas. Tech.* **2019**, *12* (10), 5303-5315.